Journal of ELECTRONIC MATERIALS
DOI: 10.1007/s11664-012-2255-7
© 2012 TMS

Effects of Bi_2Se_3 Nanoparticle Inclusions on the Microstructure and Thermoelectric Properties of Bi_2Te_3-Based Nanocomposites

HEEJIN KIM,[1,2] MI-KYUNG HAN,[1,4] CHUL-HYUN YO,[3] WOOYOUNG LEE[2,5] and SUNG-JIN KIM[1,6]

1.—Department of Chemistry and Nano Sciences, Ewha Womans University, Seoul 120-750, South Korea. 2.—Department of Materials Science and Engineering, Yonsei University, Seoul 120-749, South Korea. 3.—Department of Chemistry, Yonsei University, Seoul 130-741, South Korea. 4.—e-mail: mikihan@ewha.ac.kr. 5.—e-mail: wooyoung@yonsei.ac.kr. 6.—e-mail: sjkim@ewha.ac.kr

A series of thermoelectric nanocomposite samples were prepared by integrating Bi_2Se_3 nanoparticles into a bulk Bi_2Te_3 matrix. Primarily, spherical Bi_2Se_3 nanoparticles with diameter of ~30 nm were synthesized by combining bismuth acetate with elemental Te in oleic acid solution. Bi_2Te_3-based nanocomposite samples were prepared by consolidating the appropriate quantity of Bi_2Se_3 nanoparticles with the starting elements (Bi and Te) using typical solid-state synthetic reactions. The microstructure and composition of the Bi_2Te_3-based nanocomposites, as well as the effects of the Bi_2Se_3 nanoparticles on their thermoelectric properties, are investigated. Transmission electron microscopy observation of the Bi_2Te_3-based nanocomposites reveals two types of interface between the constituent materials, i.e., coherent and incoherent, depending on the Bi_2Se_3 concentration. The Bi_2Se_3 nanoparticles in the Bi_2Te_3 matrix act as scattering centers for a wider range of phonon frequencies, thereby reducing the thermal conductivity. As a result, the maximum ZT value of 0.75 is obtained for the Bi_2Te_3 nanocomposite with 10 wt.% Bi_2Se_3 nanoparticles at room temperature. It is clear that the reduction in the thermal conductivity plays a central role in the enhancement of the ZT value.

Key words: Bismuth telluride, thermoelectric, nanocomposite

INTRODUCTION

Thermoelectric materials which can interconvert thermal and electrical energy have been applied in many fields such as refrigeration and power generation.[1–3] The performance of a thermoelectric material can be evaluated in terms of a dimensionless figure of merit, ZT, defined as $(S^2\sigma/\kappa)T$, where S is the Seebeck coefficient, σ is the electrical conductivity, κ is the thermal conductivity, and T is the temperature in Kelvin. To maximize the ZT of a material, a large S, high σ, and low κ are required.

Since theoretical works predicted that incorporation of a nanostructured phase into a bulk material might be a promising way to obtain a significant improvement of ZT,[2–7] several groups have made progress in this direction through the development of multicomponent nanostructured thermoelectric materials. Examples are the cubic $AgPb_{18}SbTe_{20}$ material with Ag-Sb-rich nanodots in a PbTe matrix,[8] a Bi_2Te_3 nanocomposite with tubular Bi_2Te_3 nanowire inclusions,[9] $Bi_{2-x}Sb_xTe_3$-based nanocomposites with PbTe nanoparticles,[10] and a $CoSb_3$ nanocomposite with C_{60} incorporation.[11] Effective thermoelectric nanocomposites should be crystalline semiconductors that can scatter phonons without significantly interrupting the electrical conductivity. Therefore, an appropriate combination

(Received April 12, 2012; accepted August 28, 2012)

Published online: 29 September 2012

of host matrix material and nanoscale inclusions in nanocomposites is expected to be important to achieve a high ZT.[12]

Bi_2Te_3 and its alloys are the best thermoelectric materials available near room temperature with the highest ZT.[13,14] Since Bi_2Se_3 has the same crystal structure and a very small lattice mismatch with Bi_2Te_3, in this research, we synthesized Bi_2Se_3 nanoparticles and bulk Bi_2Te_3-based nanocomposites by adding Bi_2Se_3 nanoparticles during standard solid-state synthesis of Bi_2Te_3. We examine the microstructure and composition of the nanocomposites and report a systematic study of the effects of the Bi_2Se_3 nanoparticles on the thermoelectric properties of the Bi_2Te_3-based nanocomposites.

EXPERIMENTAL PROCEDURES

Bi_2Se_3 nanoparticles in sufficient quantities for integration into bulk Bi_2Te_3 material were prepared separately according to our previous report with a slight modification.[15] For the synthesis of the Bi_2Se_3 nanoparticles, 2 mmol bismuth acetate was dissolved in 20 mL oleic acid. The solution was heated to 313 K and held there for 30 min under vacuum, and a transparent solution was obtained. After flooding the solution in a flask with nitrogen, it was further heated to 373 K, and while maintaining it at this temperature, a Se-TOP solution, which had been freshly prepared by dissolving 10 mmol Se powder in 10 mL trioctylphosphine (TOP), was rapidly injected into the flask. The reaction solution changed color from clear to black immediately after the injection of the Se-TOP solution. After the reaction was allowed to proceed to completion for 1 min to 5 min, the solution was cooled to room temperature by placing the flask in a water bath and then centrifuged at 18,000 rpm for 30 min. The dark product was washed with acetone and dried in air at room temperature.

To synthesize the polycrystalline Bi_2Te_3-based nanocomposite samples, stoichiometric amounts of elemental Bi (Alfa Aesar, 99.997%) and Te (Alfa Aesar, 99.999%) for Bi_2Te_3, and a specified amount of Bi_2Se_3 nanoparticles in weight percentage (wt.%), were loaded into silica tubes (10 mm diameter, 1 mm wall thickness) and then sealed under vacuum. The sealed tubes were heated to 1273 K over a period of 12 h, held there for 12 h, slowly cooled to 673 K over a period of 12 h, and finally quenched to room temperature. A series of samples consisting of 5 wt.% and 10 wt.% Bi_2Se_3 nanoparticles in bulk Bi_2Te_3 matrix were prepared. Additionally, a Bi_2Te_3 sample without nanoparticle inclusion was prepared under identical conditions to serve as a reference.

The thermal conductivity was determined by using the thermal diffusivity, $\kappa = DC_p\rho$, where ρ, D, and C_p are the sample density, thermal diffusivity, and specific heat, respectively, of the sample. The sample density was measured by Archimedes' method and ranged from 7.0 g cm^{-1} to 7.4 g cm^{-1} at room temperature. The thermal diffusivity and specific heat were measured on Netzsch LFA-457 and DSC-404 instruments, respectively. To measure the thermal diffusivity, the samples were cut into disks with diameter of about 8 mm to 10 mm and thickness of about 2 mm. For the measurement of the electrical properties, the samples were cut into rectangular shapes with dimensions of about 3 mm × 3 mm × 10 mm. The electrical conductivity and Seebeck coefficient were measured concurrently under a low-pressure helium atmosphere from room temperature to approximately 580 K using a ULVAC-RIKO ZEM-3 instrument. The Seebeck coefficients were measured three times with different temperature gradients between 10°C and 30°C at each temperature step.

Powder x-ray diffraction (PXRD) patterns were obtained with a Rigaku x-ray diffractometer using Cu K_α radiation (λ = 1.5418 Å) at 30 mA and 40 kV. The diffraction data were recorded at scanning rate of 0.2 min^{-1}. The sample morphologies, fine structures, and selected-area electron diffraction (SAED) patterns were obtained by high-resolution transmission electron microscopy (HR-TEM; JEOL 2100F).

RESULTS AND DISCUSSION

Structural Characterization

Synthesis of Bi_2Se_3 nanoparticles was confirmed by powder XRD results. Figure 1a shows the XRD pattern of the Bi_2Se_3 nanoparticles, in which all of the peaks were indexed based on the hexagonal lattice of Bi_2Se_3 (JCPDS 33-214)[16] with $R\,\bar{3}m$(166) symmetry. No peaks for bismuth, selenium or other bismuth-selenium compounds were observed in the XRD pattern. The TEM images, shown in Fig. 1b, reveal that the Bi_2Se_3 nanoparticles are spherical in shape with average size of about 30 nm. The SAED pattern indicates that the particles are well crystallized with hexagonal symmetry. The cell parameter of the a-axis in the hexagonal lattice calculated from the SAED pattern was 4.12 Å, which is close to the unit cell parameter calculated from the powder XRD pattern. The synthesized binary Bi_2Se_3 nanoparticles were used as inclusions in the nanocomposite samples. In the applied synthesis conditions, we presume that Bi_2Se_3 was melted and recrystallized, because its melting point (980 K) is lower than our synthesis temperature (1273 K).

The Bi_2Te_3-based nanocomposite samples were characterized by powder XRD. All of the reflections in the XRD pattern in Fig. 2 can be readily indexed to the rhombohedral lattice of Bi_2Te_3 [space group: $R\,\bar{3}m$(166), JCPDS no. 15-0863],[16] except for the weak diffraction peak at $2\theta = \sim 28°$ resulting from the Bi_2Se_3 in the Bi_2Te_3 matrix. There was a slight shift in XRD peak position towards higher angle with increasing Bi_2Se_3 concentration, revealing the formation of a solid solution between Bi_2Te_3 and

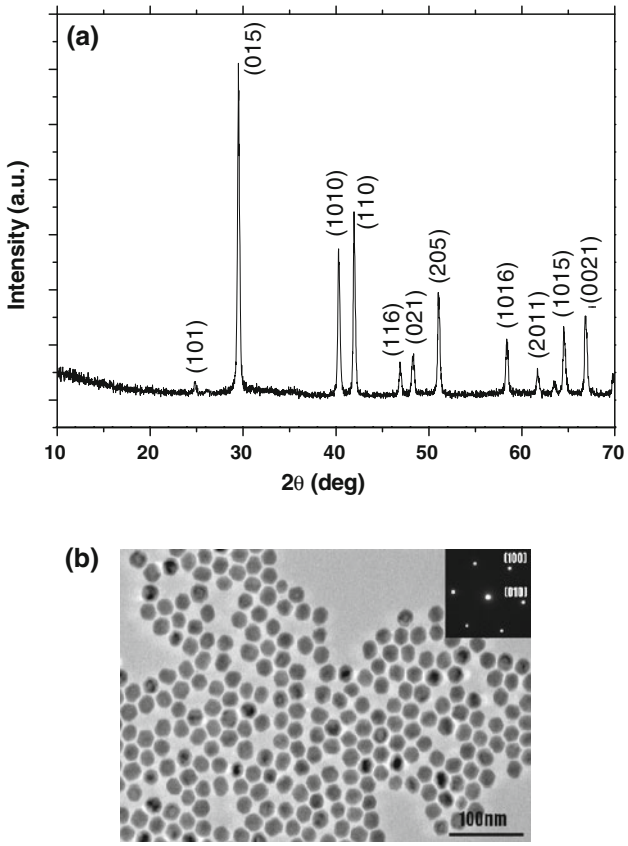

Fig. 1. (a) Powder XRD pattern of the Bi_2Se_3 nanoparticles and (b) TEM image and SAED pattern (inset: upper right) of the synthesized Bi_2Se_3 nanoparticles.

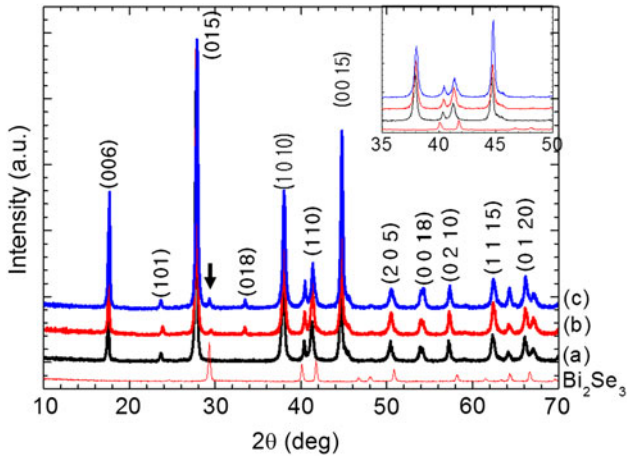

Fig. 2. Powder XRD patterns of Bi_2Te_3-based nanocomposites incorporating (a) 0 wt.%, (b) 5 wt.%, and (c) 10 wt.%, compared with the XRD pattern of synthesized Bi_2Se_3 nanoparticles. The arrow in the diffraction pattern indicates diffraction from Bi_2Se_3 in the Bi_2Te_3 matrix.

Bi_2Se_3. Since Bi_2Se_3 was melted and recrystallized in the synthesis process, some of the Se atoms substituted for Te atoms to form a $Bi_2Te_{3-x}Se_x$ solid solution and the rest of the Se atoms seem to precipitate as Bi_2Se_3 phase. Confirmation that the Bi_2Se_3 nanoparticles remain intact within the Bi_2Te_3 nanocomposites is provided by the TEM measurements. The HR-TEM and SAED images of the 5 wt.% and 10 wt.% nanocomposites are presented in Figs. 3 and 4, respectively. The presence of the Bi_2Se_3 nanoparticles was evident throughout the matrix in both cases.

Figure 3a shows a typical bright field (BF)-TEM image of the multigrains in the nanocomposite sample containing 5 wt.% Bi_2Se_3. Figure 3b shows the coherent interface between the Bi_2Se_3 particles and the Bi_2Te_3 matrix. The SAED pattern (Fig. 3b, upper right) clearly reveals the hexagonal structure without any satellite peaks, confirming the phase coherence. The size of the Bi_2Se_3 nanoparticles within the matrix was about 5 nm, as shown in Fig. 3b. No lattice distortion between the grain matrix and the nanoparticles was observed, indicating the existence of a coherent interface. This coherent interface is not expected to influence the electron transfer, but would impede thermal conduction via phonon scattering.

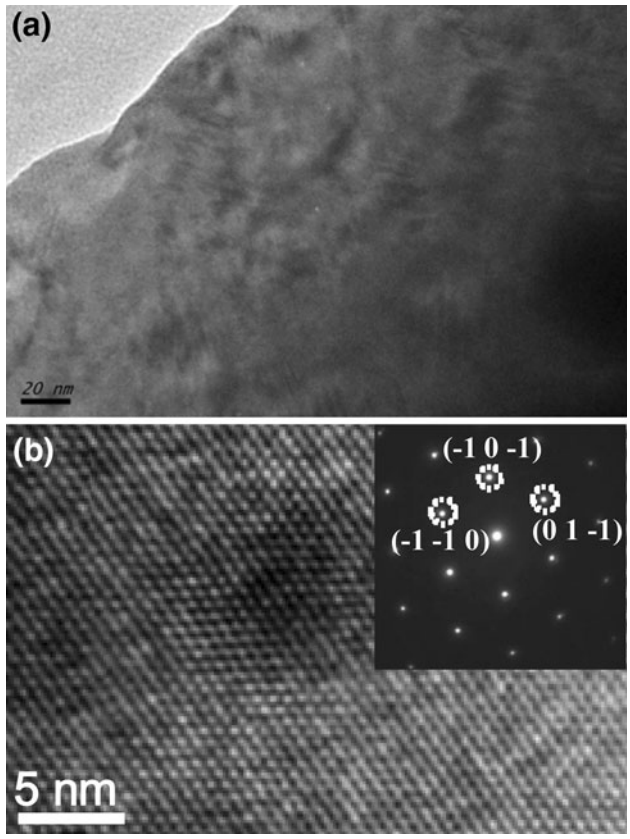

Fig. 3. (a) Bright field (BF)-TEM image of multigrains and SAED pattern of 5 wt.% Bi_2Se_3 sample, and (b) HR-TEM image and SAED pattern (inset: upper right) of Bi_2Se_3 nanoparticles (under ~5 nm) embedded in the grain matrix.

Figure 4a shows a typical BF-TEM image of the multigrains in the 10 wt.% Bi_2Se_3 nanocomposite sample. The low-magnification TEM image of the

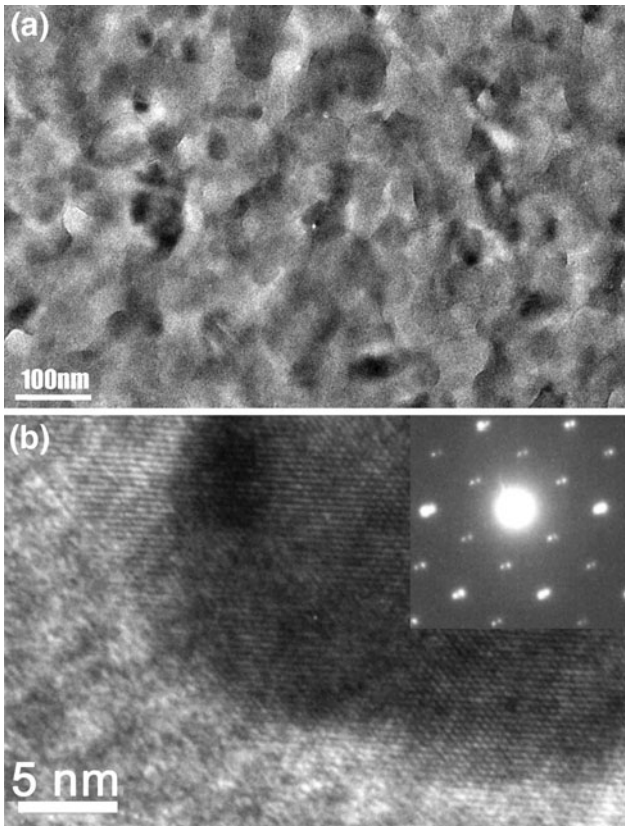

Fig. 4. (a) BF-TEM image of 10 wt.% Bi_2Se_3 sample, and (b) dark field (DF)-TEM image and SAED pattern (inset: upper right) of the interface between the Bi_2Se_3 nanoparticles (~20 nm) and the matrix.

sample shows that the embedded nanoparticles are evenly dispersed within the matrix. Figure 4b indicates that the interfaces between the Bi_2Se_3 nanoparticles and the Bi_2Te_3 matrix are incoherent. The SAED pattern (upper right in Fig. 4b) shows satellite peaks, which were attributed to the Bi_2Te_3 and Bi_2Se_3 phases. These incoherent boundaries are known to scatter not only phonons, but also electrons. From the TEM observation of Bi_2Te_3 bulk nanocomposite with Bi_2Se_3 nanoparticles, we note that two types of interface exist in the matrix depending on the Bi_2Se_3 concentration. The effects of the Bi_2Se_3 nanoparticles incorporated in the Bi_2Te_3 matrix on the charge transport properties of the Bi_2Te_3-based nanocomposites are discussed in the following section.

Thermoelectric Transport Properties

Hall measurements were carried out at room temperature. The Hall coefficients are negative, indicating n-type conduction, in agreement with the Seebeck coefficient measurements. Stoichiometric bismuth telluride is p-type with free carrier concentration of approximately 10^{19} cm^{-3}. Some room-temperature Hall properties of the 0 wt.%, 5 wt.%, and 10 wt.% samples in comparison with that of commercial Bi_2Te_3 are listed in Table I. The measured carrier concentration of the 10 wt.% Bi_2Se_3 sample is approximately 2.72×10^{19} cm^{-3}, which is slightly higher than that of the 5 wt.% Bi_2Se_3 sample (Table I). The large carrier concentration in the 10 wt.% Bi_2Se_3 sample is consistent with the lower Seebeck coefficient in this sample.

Figure 5 illustrates the dependence of the thermoelectric properties on the concentration of Bi_2Se_3 nanoparticles embedded in the Bi_2Te_3-based nanocomposites. All of the properties were measured in the same direction. The temperature dependence of the electrical conductivity, σ, is shown in Fig. 5a. In all cases, the electrical conductivity decreases with increasing temperature over the measured temperature range, indicating degenerate semiconducting behavior. The electrical conductivity of the nanocomposite samples decreases with increasing Bi_2Se_3 nanoparticle content. The result for the 10 wt.% sample shows a relatively low electrical conductivity (~85 S/cm at room temperature). This may be caused by the inhomogeneity of the Bi_2Se_3 nanoparticles within the matrix. We supposed that the interface between the matrix and the particles interrupted the electron transfer and the interface of the 10 wt.% Bi_2Se_3 sample exerted a particularly strong influence on the electron transfer above 450 K.

Figure 5b presents the temperature dependence of the Seebeck coefficient of the nanocomposite samples. The Seebeck coefficient is negative across the whole temperature range, indicating that the majority of charge carriers are electrons (n-type). As the temperature increases, the magnitude of the Seebeck coefficient of the samples decreases. The Seebeck coefficient for the 5 wt.% sample ranges from approximately -140 μV/K at room temperature to approximately -105 μV/K at 580 K, whereas for the 10 wt.% sample it ranged from approximately -148 μV/K at room temperature to approximately -120 μV/K at 580 K.

The electrical conductivity and Seebeck coefficient values were used to calculate the power factor, $S^2\sigma$, as shown in Fig. 5c. The reference 0 wt.% Bi_2Se_3 sample showed a maximum power factor of ~24 μW/cm K^2 at room temperature. For all samples, the power factor steadily decreases with increasing temperature. The 5 wt.% Bi_2Se_3 sample shows lower power factors than the 10 wt.% Bi_2Se_3 sample due to its smaller Seebeck coefficient. The highest value of the power factor (19 μW/cm K^2) was obtained for the 10 wt.% Bi_2Se_3 sample at room temperature.

The effect of these nanoscale inhomogeneities on the heat transport in these materials was studied by thermal diffusivity measurements as a function of temperature. Figure 5d shows the temperature dependence of the total thermal conductivity of the 0 wt.% (reference sample), 5 wt.%, and 10 wt.% Bi_2Se_3 samples. As expected, the total thermal conductivity decreases upon the addition of the Bi_2Se_3 nanoparticles. The total thermal conductivity,

Table I. Hall-effect transport properties of the 0 wt.%, 5 wt.%, and 10 wt.% samples at room temperature

Sample	R_H ($cm^3\ C^{-1}$)	Carrier Concentration ($10^{19}\ cm^{-3}$)	Mobility ($cm^2\ V^{-1}\ s^{-1}$)
0 wt.%	−0.405	1.54	277
5 wt.%	−0.346	1.80	211
10 wt.%	−0.229	2.72	168
Commercial Bi_2Te_3 ingot[12]		1.8 (p-type)	255 (c-direction)

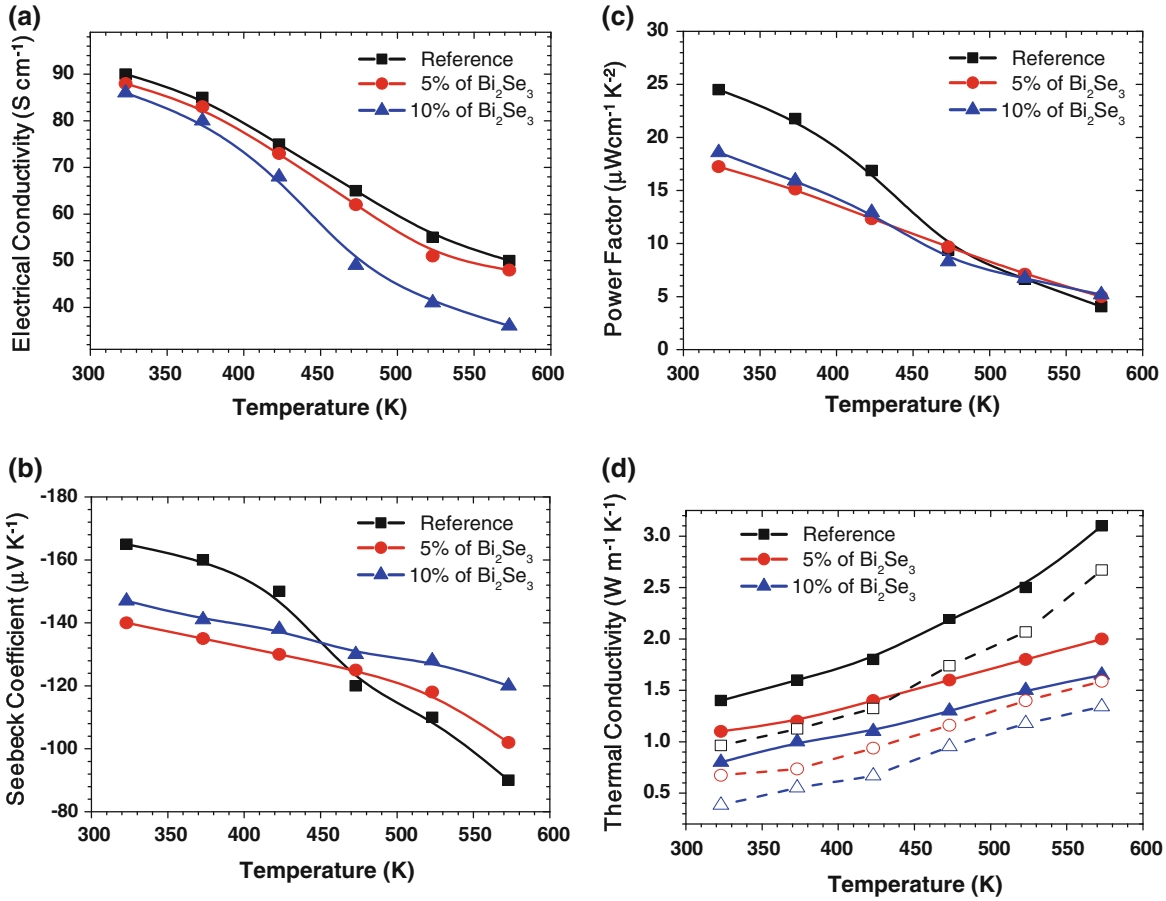

Fig. 5. Temperature dependence of (a) electrical conductivity, (b) Seebeck coefficient, (c) power factor, and (d) total thermal conductivity of 0 wt.% (reference), 5 wt.%, and 10 wt.% Bi_2Se_3 samples. The dashed line in (d) indicates the phonon contribution to the thermal conductivity. The measurement uncertainty on individual samples is approximately 30%, 7%, and 30% for σ, S, and κ, respectively.

κ, consists of the phonon contribution, κ_{ph}, and the carrier contribution, κ_e, which is related to the electrical conductivity, σ, by the relation $\kappa_e = L_0\sigma T$, where L_0 is the Lorenz number ($L_0 = 1.53 \times 10^{-8}$ $V^2\ K^{-2}$).[17] The dashed line in Fig. 5d shows the phonon contribution to the total thermal conductivity. The κ_{ph} values of the 5 wt.% and 10 wt.% samples at 300 K are ~0.7 W/m K and ~0.4 W/m K, respectively. These values are smaller than that of the reference 0 wt.% Bi_2Se_3 sample (κ_{ph} value ~1.0 W/m K at room temperature). It seems that the atomic structural disorder due to the formation of a solid solution between the Bi_2Se_3 nanoparticles and Bi_2Te_3 matrix is essentially responsible for these low values. Furthermore, the considerable reduction of the thermal conductivity observed in the Bi_2Te_3 bulk nanocomposite with 10 wt.% Bi_2Se_3 nanoparticles seems to be due to the coexistence of coherent and incoherent interfaces which scatter a wider range of phonon frequencies. It is clear from these results that incorporation of the Bi_2Se_3 nanoparticles within the Bi_2Te_3 matrix causes a significant decrease in the lattice thermal conductivity.

Figure 6 shows the temperature dependence of ZT for the 0 wt.% (reference), 5 wt.%, and 10 wt.% Bi_2Se_3 samples. It can be seen that the value of ZT decreases monotonically with increasing

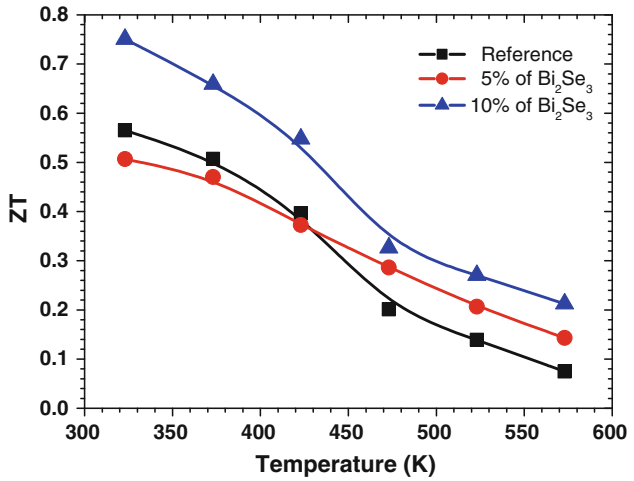

Fig. 6. Temperature dependence of the dimensionless figure of merit for the 0 wt.% (reference), 5 wt.%, and 10 wt.% Bi_2Se_3 samples.

temperature. The highest *ZT* values were 0.75 and 0.50 for the 10 wt.% and 5 wt.% samples at room temperature. The *ZT* of the 5 wt.% sample was lower than that of the reference 0 wt.% Bi_2Se_3 sample below 423 K, but higher at temperatures above 423 K, which is mainly related to the phonon contribution to the thermal conductivity. The maximal *ZT* at room temperature for the 10 wt.% sample was about 40% higher than that of the reference 0 wt.% Bi_2Se_3 sample. We suppose that the phonon contribution to the thermal conductivity is the important factor in the high-temperature region. It is clear from these results that the incoherent interfaces cause a significant decrease in the thermal conductivity without causing a significant reduction in the electrical conductivity. Therefore, controlling the interface is a highly effective way of enhancing the thermoelectric properties.

CONCLUSIONS

Synthesis of spherical Bi_2Se_3 nanoparticles with average diameter of 30 nm was successfully accomplished. Bi_2Te_3-based nanocomposites were prepared by incorporating 0 wt.%, 5 wt.%, and 10 wt.% Bi_2Se_3 nanoparticles into a Bi_2Te_3 matrix. The microstructural analysis results suggested that the proper amount of Bi_2Se_3 particles in the matrix induced both coherent and incoherent interfaces in the composite. The incoherent interfaces which increased with increasing Bi_2Se_3 particle content cause a significant decrease in the thermal conductivity without any significant change in the electrical conductivity. The maximum *ZT* of 0.75 are observed for the Bi_2Te_3 bulk with 10 wt.% Bi_2Se_3 nanoparticles at room temperature. It is clear that the reduction of the thermal conductivity plays a central role in the enhancement of *ZT*.

ACKNOWLEDGEMENTS

This work was supported by the Basic Science Research Program through the National Research Foundation of Korea (20110003767), Nano Material Technology Development Program through the National Research Foundation of Korea (NRF) funded by the Ministry of Education, Science, and Technology (20110030147), and "Center for Nanostructured Materials Technology" under "21st Century Frontier R&D Programs" of the Ministry of Education, Science, and Technology, Korea (2011K000197). Prof. Yo acknowledges financial support from the KISTI ReSEAT Program, Korea.

REFERENCES

1. L.E. Bell, *Science* 321, 1457 (2008).
2. M.G. Kanatzidis, *Chem. Mater.* 22, 648 (2010).
3. G.J. Snyder and E.S. Toberer, *Nat. Mater.* 7, 105 (2008).
4. A. Minnich and G. Chen, *Appl. Phys. Lett.* 91, 073105 (2007).
5. T.M. Tritt, ed., *Semiconductor and Semimetals*, vol. 71 (San Diego: Academic, 2001).
6. R.G. Yang and G. Chen, *Phys. Rev. B* 69, 195316 (2004).
7. D.J. Bergman and L.G. Fel, *J. Appl. Phys.* 85, 8205 (1999).
8. K.F. Hsu, S. Loo, F. Guo, W. Chen, J.S. Dyck, C. Uher, T. Hogan, E.K. Polychroniadis, and M.G. Kanatzidis, *Science* 303, 818 (2004).
9. X.B. Zhao, X.H. Ji, Y.H. Zhang, T.J. Zhy, J.P. Tu, and X.B. Zhang, *Appl. Phys. Lett.* 86, 062111 (2005).
10. S. Ganguly, C. Zhou, D. Morelli, J. Sakamoto, C. Uher, and S.L. Brock, *J. Solid State Chem.* 184, 3195 (2011).
11. X. Shi, L. Chen, J. Yang, and G.P. Meisner, *Appl. Phys. Lett.* 84, 2301 (2004).
12. C.J. Vineis, A. Shakouri, A. Majumdar, and M.G. Kanatzidis, *Adv. Mater.* 22, 3970 (2010).
13. F.J. DiSalvo, *Science* 285, 703 (1999).
14. Y. Ma, Q. Hao, B. Poudel, Y. Lan, B. Yu, D. Wang, G. Chen, and Z. Ren, *Nano Lett.* 8, 2580 (2008).
15. H.J. Kim, K.J. Lee, S.-J. Kim, and M.-K. Han, *Bull. Korean Chem. Soc.* 31, 1123 (2010).
16. W. McClune, *Powder Diffraction File* (Swarthmore, PA: JCPDS International Center for Diffraction Data, 1997).
17. L.D. Hicks and M.S. Dresselhaus, *Phys. Rev. B* 47, 12727 (1993).